JOURNAL OF GEOPHYSICAL RESEARCH, VOL. 106, NO. D20, PAGES 24,315–24,333, OCTOBER 27, 2001

Nighttime observations of anomalously high levels of hydroxyl radicals above a deciduous forest canopy

Ian Faloona,[1,2] Dave Tan,[1,3] William Brune,[1] Julia Hurst,[4] Dennis Barket Jr.,[4] Tara L. Couch,[4] Paul Shepson,[4] Eric Apel,[5] Daniel Riemer,[5,6] Troy Thornberry,[7] Mary Anne Carroll,[7] Sanford Sillman,[7] Gerald J. Keeler,[7] Jessica Sagady,[8] Dianne Hooper,[8] and Kurt Paterson[8]

Abstract. Diurnal measurements of hydroxyl and hydroperoxy radicals (OH and HO_2) made during the Program for Research on Oxidants: Photochemistry, Emissions, and Transport (PROPHET) summer intensive of 1998 indicate that these key components of gas phase atmospheric oxidation are sustained in significant amounts throughout the night in this northern forested region. Typical overnight levels of OH observed were 0.04 parts per trillion (pptv) (1.1×10^6 molecules/cm^3), while HO_2 concentrations ranged from 1 to 4 pptv. Results of diagnostic testing performed before, after, and during the deployment suggest little possibility of interferences in the measurements. Collocated measurements of the reactive biogenic hydrocarbon isoprene corroborate the observed levels of OH by exhibiting significant decays overnight above the forest canopy. The observed isoprene lifetimes ranged from 1.5 to 12 hours in the dark, and they correlate well to those expected from chemical oxidation by the measured OH abundances. Possible dark reactions that could generate such elevated levels of OH include the ozonolysis of extremely reactive biogenic terpenoids. However, in steady state models, which include this hypothetical production mechanism, HO_2 radicals are generated in greater quantities than were measured. Nonetheless, if the measurements are representative of the nocturnal boundary layer in midlatitude temperate forests, this observed nocturnal phenomenon might considerably alter our understanding of the diurnal pattern of atmospheric oxidation in such pristine, low-NO_x environments.

1. Introduction

Most of the photochemical processing of trace gases in the atmosphere is thought to occur during the daylight hours when sufficient luminant energy is available for the photolytic production of extremely reactive species like the hydroxyl and hydroperoxy radicals (OH and HO_2, collectively referred to as HO_x). These short-lived molecules react rapidly (in the case of OH) with the myriad array of hydrocarbons in the lower atmosphere, with each other, and with oxides of nitrogen; and are thereby intimately linked to the in situ chemical formation of ozone in the troposphere. Because of their extreme reactivity, these odd-hydrogen radicals have traditionally been believed to decay rapidly in the dark as their primary photolytic sources disappear and continuing chemistry consumes them. At night chemical oxidation (of, for example, reactive hydrocarbons) is thought to be carried out principally by the nitrate radical (NO_3) [*Wayne et al.*, 1991; *Platt et al.*, 1990; *Aliwell and Jones*, 1998]. Rapidly photolyzed at wavelengths below 620 nm, nitrate radicals possess lifetimes which increase from a few seconds in the daylight hours to several minutes at night [*Smith et al.*, 1995].

Although the two main daytime OH sources

(R1) $$O_3 + h\nu(\lambda<320\text{ nm}) \rightarrow O(^1D) + O_2$$
$$O(^1D) + H_2O \rightarrow 2OH$$

and

(R2) $$HCHO + h\nu(\lambda<340\text{ nm}) \rightarrow H + CHO$$
$$H + CHO + 2O_2 \rightarrow 2HO_2 + CO$$

followed by

(R3) $$HO_2 + NO \rightarrow OH + NO_2$$

vanish at night, there are other nonzero sources that are known to produce finite amounts of OH in the dark. Past modeling studies have tried to estimate the relative contributions of OH and NO_3 overnight for various environmental conditions [*Platt et al.*, 1990; *Bey et al.*, 1997]. The models tend to confirm the suspicion that nitrate is the premier nocturnal oxidant throughout the troposphere. In fact, some conditions have been found in which total

[1]Department of Meteorology, The Pennsylvania State University, University Park, Pennsylvania.
[2]Now at National Center for Atmospheric Research, Boulder, Colorado.
[3]Now at School of Earth and Atmospheric Sciences, Georgia Institute of Technology, Atlanta, Georgia.
[4]Department of Chemistry, Purdue University, West Lafayette, Indiana.
[5]National Center for Atmospheric Research, Boulder, Colorado.
[6]Now at Rosenstiel School of Marine & Atmospheric Science, University of Miami, Miami, Florida.
[7]Atmospheric, Oceanic, and Space Sciences Department, University of Michigan, Ann Arbor, Michigan.
[8]Department of Civil and Environmental Engineering, Michigan Technological University, Houghton, Michigan.

Copyright 2001 by the American Geophysical Union.

Paper number 2000JD900691.
0148-0227/01/2000JD900691$09.00

nighttime nitrate oxidation is on par with total OH oxidation (assumed to occur predominantly in the day) of olefins, terpenes, many aromatics, and some sulfur compounds [*Wayne et al.*, 1991; *Smith et al.*, 1995]. However, recent experiments conducted in low-NO_x forested environments have demonstrated various signs of rapid chemical oxidation taking place in the dark [*Goldan et al.*, 1995; *Biesenthal et al.*, 1998; *Leaitch et al.*, 1999] which are inexplicable by conventional schemes of nighttime atmospheric chemistry. This paper examines the nighttime chemistry at a forest site in northern Michigan, as it pertains to the observed levels of HO_x, through analysis of a wide range of chemical and micrometeorological data collected during July and August 1998.

2. Experimental Descriptions

2.1. PROPHET Forest Research Site

The Program for Research on Oxidants: Photochemistry, Emissions, and Transport (PROPHET) is a collaborative research venture operated at a forested tower site in the vicinity of the University of Michigan Biological Station (UMBS) [*Carroll et al.*, this issue]. The UMBS is located on the southern shore of Douglas Lake approximately 20 km east of Pellston, Michigan (45°33′33″N, 84°42′53″W). The site is central to the Great Lakes Region and as such is ideal for studying air chemistry under a broad range of environmental conditions, including pristine continental air from central Canada, mixed air masses of biogenic and anthropogenic influence, and fully impacted urban plumes from midwestern industrial centers such as Chicago, Milwaukee, and Detroit [*Cooper et al.*, this issue]. Located 25 km south of the Straits of Mackinac, 30 km east of Lake Michigan, and 50 km west of Lake Huron, the experimental site is locally characterized by biogenic volatile organic compound (VOC) emissions, which dominate those from anthropogenic sources [*Sumner et al.*, this issue]. A complete description of the site location and climatology may be found in the works of *Carroll et al.* [this issue] and *Cooper et al.* [this issue].

2.2. Tower-Sampling Instrumentation

Air sampling was carried out atop a 31 m permanent tower laboratory that rises approximately 10 m above the mean canopy top. The canopy is one of a mixed hardwood forest constituted mostly of aspen, maple, and beech species. The measurements of HO_x, NO_y, and large aerosols were made at the top platform of the tower, but all other samples are carried to an environmentally controlled laboratory at the base of the tower through a 5 cm ID Pyrex sampling inlet from a height of 35 m. A high-volume blower delivers air from the top of the tower to the laboratory instrumentation in less than 2 s at a flow rate of 3300 liters per minute (LPM). The exhaust from this system and all other instrument pumps was diverted underground to a fenced-off venting area 40 m to the east near the access road.

Measurements of isoprene and its first-generation oxidation products, methacrolein (MACR), methyl vinyl ketone (MVK), and 3-methylfuran (MFUR) were made by both the Purdue and the NCAR groups using gas chromatographic (GC) separation followed by mass spectrometric (MS) identification. The Purdue system delivers air from the manifold to a Tenax TA adsorbant (maintained at ~283 K) via a 6.4 mm PFA Teflon sampling line for 5 min at a time. The sample is then thermally desorbed at 525 K into a Poraplot column followed by mass spectrometric detection using a HP 5972 mass selective detector. The estimated limit of detection for the reported 40 min isoprene data is 15 parts per trillion by volume (pptv) [*Barket et al.*, this issue]. The Purdue instrument made overnight measurements on 24 evenings in the period from Julian day (JD) 194, July 13, to JD 227, August 15.

The NCAR instrument made measurements of isoprene and the above mentioned oxidation products, in addition to α- and β-pinene and eight other monoterpenes. The instrumental method was similar to that of Purdue with the following exceptions: A 300 mL sample (about a 3 min sampling duration) was dried in a 263 K Silcosteel tube and then concentrated onto a glass bead trap at 130 K. The sample is then injected into an HP-624 capillary column (60 m x 0.25 mm ID x 1.4 mm film). Electron impact mass spectrometry operated in a single ion monitoring mode was used for quantification and a 3 min sample was run every 30 min. The limit of detection for this instrument is estimated at 1 pptv with an absolute accuracy based on propagation of errors through the calibration process of 6%. The instrument was on line for a subset of the entire field intensive, recording only seven overnight periods from JD 217, August 5, to JD 225, August 13.

The NO_x measurements were made by a custom-built NO-O_3 chemiluminescence instrument. The 2σ detection limit in 1 min was 1.3 pptv, and the estimated uncertainty in the NO was ±(19% + 2 pptv) [*Thornberry et al.*, this issue]. The aerosol data used in this analysis is a hybrid from two instruments. The first is a TSI scanning mobility particle sizer (SMPS), which was operated under conditions allowing for quantification of ultrafine aerosols with diameters between 5 and 185 nm with an estimated uncertainty of 1.0-2.5% in diameter. A TSI APS3320 time-of-flight counter was used to measure particles in the size range between about 0.35 and 20 μm aerodynamic diameter. An RM Young propeller anemometer/vane was mounted at the top of the tower directly above the opening of the inlet manifold at a height of 35 m above the forest floor (approximately 14 m above the mean canopy height).

All of the measurements used in this analysis were merged into a common 30 min time series (the averaging period used by the HO_x measurements) for the entire 7 week campaign. The most appropriate time coordinate for a photochemical study is local mean solar time, and it is used throughout the following analysis. On average, local mean solar time was 5 hours and 40 min behind Greenwich meridian time, or 1 hour and 40 min behind eastern daylight time (local time) during the 7 week intensive. In our modeling analysis, observations of isoprene, which fell below the instrumental limit of detection, were set to one-half the limit value. Such low isoprene concentrations were recorded by the Purdue instrument on less than 6% of the total nocturnal measurements, and none of these data was included in the intervals of the forthcoming decay analysis.

2.3. HO_x Instrument

The OH and HO_2 radical measurements were made with the Penn State ground-based tropospheric hydrogen oxides sensor (GTHOS) instrument which is based on laser-induced

fluorescence (LIF) of the OH molecule. The same instrument in a slightly different configuration, airborne tropospheric hydrogen oxides sensor (ATHOS), has been deployed in three aircraft experiments aboard the NASA DC-8 airborne laboratory [*Brune et al.*, 1997; *Faloona et al.*, 2000]. The main difference between the two configurations is that the detection module of the ground-based sensor is mounted on top of the tower contained in a thin sheet-metal enclosure (56 x 66 x 46 cm), while the laser and data acquisition system are housed inside the laboratory located at the base of the tower. Such a separation was necessary to maintain a brief interval between sample intake and detection (approximately 10 ms) while keeping the environmental conditions around the laser and data recording electronics relatively constant. The OH detection method is that of *Hard et al.* [1984], wherein an air sample is expanded through a pinhole inlet (1.1 mm) into a reduced pressure detection chamber, and the OH molecules are excited by spectrally narrow (~3 GHz full width half maximum (FWHM)) laser pulses (3 kHz) at one of several rovibronic transition lines near 308 nm ($A^2\Sigma$-$X^2\Pi$, v'=0←v"=0). The UV laser beam was delivered to the detection module on top of the tower from the lab via a 41 m, 0.365 mm diameter optical fiber waveguide (ThorLabs, Newton, New Jersey). After each laser pulse clears the detection chamber, fast switching electronics bias the microchannel plate detector (Hamamatsu, Bridgewater, New Jersey) into a high gain state, and the photons from the fluorescing OH molecules in the sample are counted. While passing from the first to a second, identical detection chamber, the sample is titrated with NO (nitric oxide, >99% Matheson, Twinsburg, Ohio) to quantitatively convert the HO_2 to OH (R3), and in this way HO_2 is measured simultaneously. A description of the prototype instrument may be found in the works of *Stevens et al.* [1994], and a comprehensive instrumental description of ATHOS and GTHOS is in preparation by W. H. Brune et al. (2001).

2.3.1. Calibration. GTHOS was automated so that unattended data collection could continue for up to 24 hours. Every hour on the half-hour the control system initiated an automatic diagnostic sequence in which various facets of instrument performance were evaluated. During this 8 min interval the NO titration flow was tested for maximum conversion of HO_2 to OH, C_3F_6 was injected upstream of the detection chambers to selectively remove the ambient OH from the sample and thereby establish an instrumental baseline [*Dubey et al.*, 1996], and the laser was blocked with a shutter to keep track of the offsets on the photodiodes that monitor the laser power at various positions in the system.

On three separate occasions the instrumental calibration system was brought to the top of the tower for in-field calibrations. Ultra-zero-compressed air was run from the base of the tower up to the calibration system, and variable slipstream flows were passed through a deionized water bubbler. The water content in the resultant mixture was monitored by a LICOR LI-6969 H_2O/CO_2 instrument (LICOR Instruments, Lincoln, Nebraska), an IR absorption spectrometer with a linear response from tens of parts per million by volume (ppmv) concentrations up to water saturation values of ~2.5%. Two low-pressure Hg lamps, whose specific 184.9 nm flux output has been well characterized in the lab as a function of lamp power supply current, provide the energy for H_2O photolysis in a 2.5 x 1.2 cm irradiation region at the outlet of the calibration system. Careful measurement of the flow rate (>40 SLPM), 185 nm integrated actinic flux, and water vapor concentration is used in conjunction with the photolysis cross section of water [*Cantrell et al.*, 1997] to determine the quantity of HO_x produced by the following reactions that take place at ambient conditions within the calibrator:

Table 1. GTHOS Calibration History for PROPHET 1998 Deployment

Calibration Date	Sensitivity (Counts/s/pptv/mW)			
	OH	σ	HO_2	σ
Premission				
07/06/98	32.5	2.2	24.5	3.3
On tower				
07/25/98	32.2	3.5	20.4	2.2
07/27/98	30.0	0.9	21.5	0.6
08/08/98	27.5	3.0	23.7	N/A
Postmission				
09/21/98	32.5	0.7	N/A	N/A
09/23/98	31.6	2.7	N/A	N/A
10/13/98	33.9	2.5	N/A	N/A
Weighted ave.	31.6		21.5	

Read 07/06/98 as July 6, 1998.

(R4) $H_2O + h\nu\ (\lambda=185\ \text{nm}) \rightarrow H + OH$
$H + O_2 \rightarrow HO_2$.

Care had to be taken in delivering the calibration air to the GTHOS inlet because the winds at the top of the tower were often intrusive. Data reduction indicated that many of the calibration points had been vitiated by the ambient air and these points were discarded from the calibration data. Table 1 shows the instrument sensitivities as measured in the lab before and after the deployment, as well as the three tower calibrations. The sensitivity is reported in terms of photon counts per second measured per pptv of analyte normalized to 1 mW of UV laser power measured at the exit of the detection axis. Currently, the upper limit of the absolute uncertainty in the calibration technique is estimated at ± 40% (at 95% confidence), but great care is taken to make sure that none of the parameters associated with these uncertainties drift over the duration of a given field deployment. Therefore such a conservative estimate of uncertainty is not representative of the overall instrument precision, which is primarily governed by system performance and sample integration time. Further discussion of the specific calibration procedures for the Penn State HO_x instrument is forestalled to a soon to be submitted paper.

2.3.2. Possible artifacts. Early attempts to measure OH by LIF were plagued by artifacts of the instrumental detection process [*Eisele and Bradshaw*, 1993]. Photolysis of ozone within the detection chamber can lead to the generation of OH (R1) and subsequent measurement of the spurious analyte. The problem has been alleviated in more recent versions of the technique by using the OH absorption feature at 308 nm, instead of 282 nm, where the photolysis cross section of O_3 is some 30 times smaller. Previous laboratory tests of ATHOS, the airborne version of the Penn State HO_x instrument, with zero air, ozone, and water vapor have shown that no

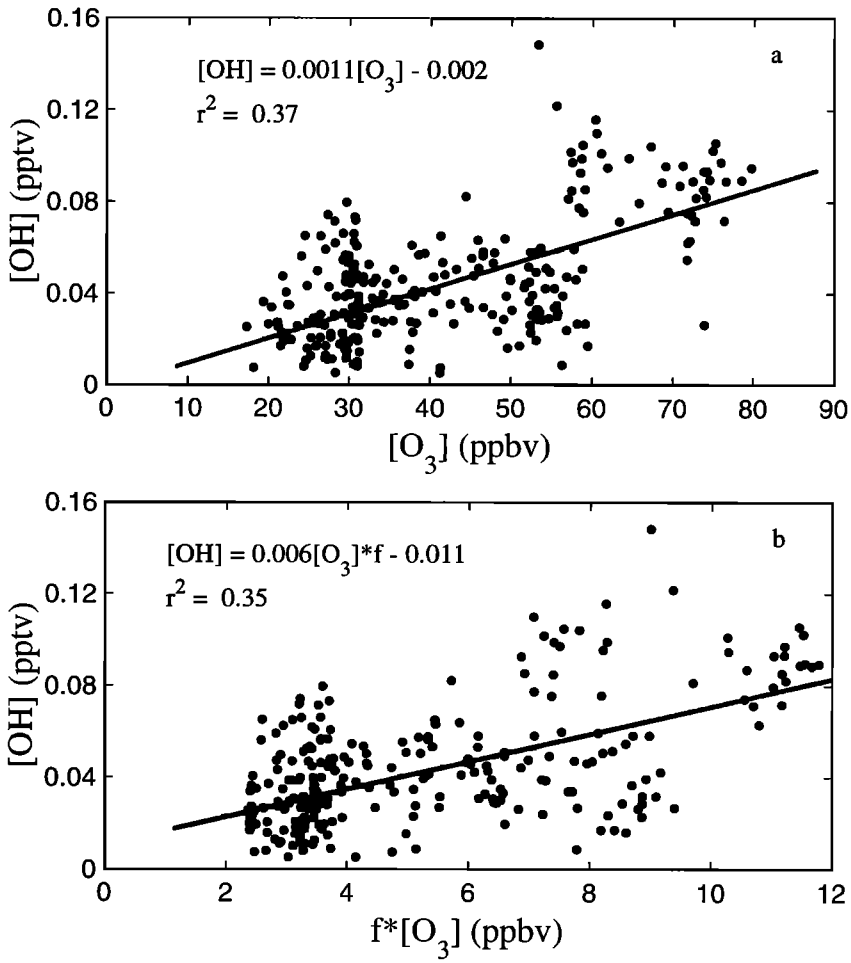

Figure 1. (a) Scatterplot of 30 min OH and O_3 measurements made during the nighttime hours (defined by UV-B flux equal to zero) and (b) similar plot of [OH] versus the product of $f*[O_3]$. The latter represents the probability of ambient ozone generating a signal within the laser induced fluorescence (LIF) instrument by laser photolysis followed by reaction with ambient moisture. The solid lines are least squares linear regressions of the data points.

discernable OH signal is generated under typical tropospheric conditions (i.e., $[O_3]$<600 ppbv). Further laboratory testing involving HCHO, H_2O_2, HONO, and SO_2 have indicated the absence of chemical interferences from these species as well. Because of the need for the airborne sampling to take place well away from the fluid surface layer around the fuselage, the inlet tube on ATHOS is 4 times longer than the one used on the tower in Michigan. Given that the ozone testing was performed with this longer inlet tube, it seems less likely that any undisclosed ozone/surface dark reaction could be creating OH internally during the PROPHET study. Still, the possibility exists that such a phenomenon, or some unknown photochemical process, is taking place inside the instrument.

The correlation between measured nighttime OH and the ambient ozone concentrations is illustrated in Figure 1a. This is not necessarily indicative of an interfering mechanism, however, because it is very natural for the two related oxidants to be correlated in the atmosphere. Ozone is an OH precursor in the daytime and nighttime troposphere as will be discussed later. A more direct measure of the interference potential from the above mentioned mechanism (R1) is the product of the ozone concentration and f, the branching ratio of $O(^1D)$ to form OH relative to its collisional deactivation by air. This parameter is proportional to the water vapor mixing ratio q as

$$f = (k_1.*q)/(k_{N2}*0.8+k_{O2}*0.2+k_1.*q), \quad (1)$$

where k_1 is the reaction (R1) rate coefficient of $O(^1D)$ with H_2O, and k_{N2} and k_{O2} are the quenching rate coefficients for $O(^1D)$ with nitrogen and oxygen, respectively [*DeMore et al.*, 1997]. The relationship between nighttime OH and the product $f*[O_3]$ is shown in Figure 1b, and it does not correlate any better than with ozone alone (Figure 1a).

Aside from the routine perfluoropropene (C_3F_6) tests that took place for brief periods during the diagnostic sequences, we ran extended tests late in the night to probe the nature of the sizable nighttime signal. C_3F_6 reacts very rapidly and selectively with OH [*Stevens et al.*, 1994], therefore it is introduced inside the instrument to confirm that the signal is derived from hydroxyl radicals and not from laser-generated artifacts [*Dubey et al.*, 1996]. The lifetime of OH with respect to C_3F_6 under the operating conditions within the instrument is approximately 1 ms, and the reactant is allowed to mix into the airstream for 5-8 ms prior to detection thus removing most of the ambient OH. If any OH were generated within the laser pulse, a maximum of ~25% of it would have a

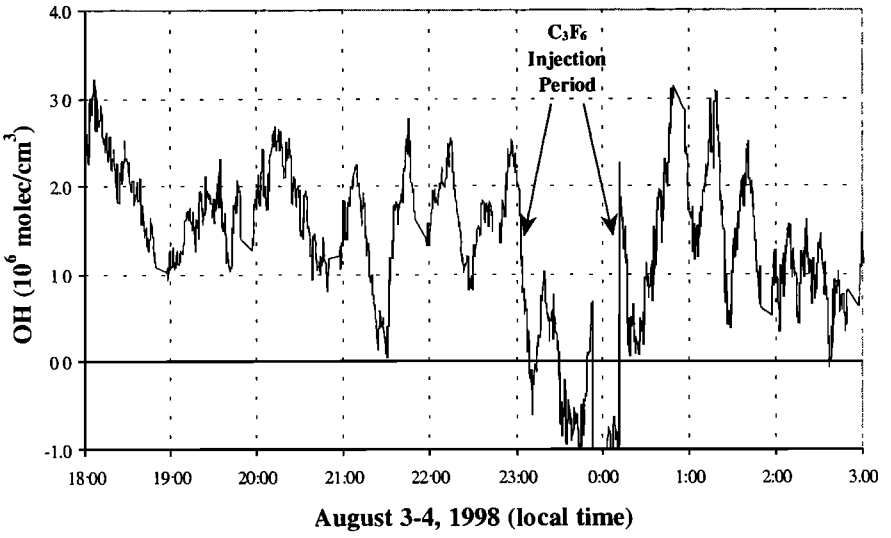

Figure 2. Time series of 15 min running average [OH] ($\div 10^6$ molecules/cm^3) over the course of August 3-4, 1998, during which a perfluoropropene interference test was performed (shaded area).

chance to react with C_3F_6 before the next pulse 333 μs later. Figure 2 shows a 15 min running average of 20 s OH data measured on August 3–4, 1998. From 1107 to 0014, C_3F_6 was injected upstream of the OH detection axis, and the average concentration measured for this interval was -1.1×10^5 molecules/cm^3. The estimated 1σ precision of the 67 min integration period is approximately 3×10^5 molecules/cm^3, so the signal is effectively zero within the noise limitations of the measurement.

Further evidence of the absence of artificial signals comes in the form of zero-air tests performed on the tower and extensively in the lab after the experiment. The tests illustrated in Figure 3 were conducted with ultra high purity zero air from two different manufacturers and several different production batches. The zero air is fed to the instrument for 25 to 70 min, and the error bars in the figure denote the 1σ precision appropriate for the duration and operating parameters of each test. Most of these tests generate signals within 1σ of zero with the exception of test number 3 which falls within 2σ. The results indicate an absence of unexpected statistical biases in the instrumental technique that might lead to spurious signals.

While the ambient OH measurements never reach within 1σ of zero for any considerable duration throughout the PROPHET campaign, there are examples from several other deployments in which an effective zero was registered by the Penn State HO_x instrument. One such example from the Southern Oxidant Study at Cornelia Fort airport outside of

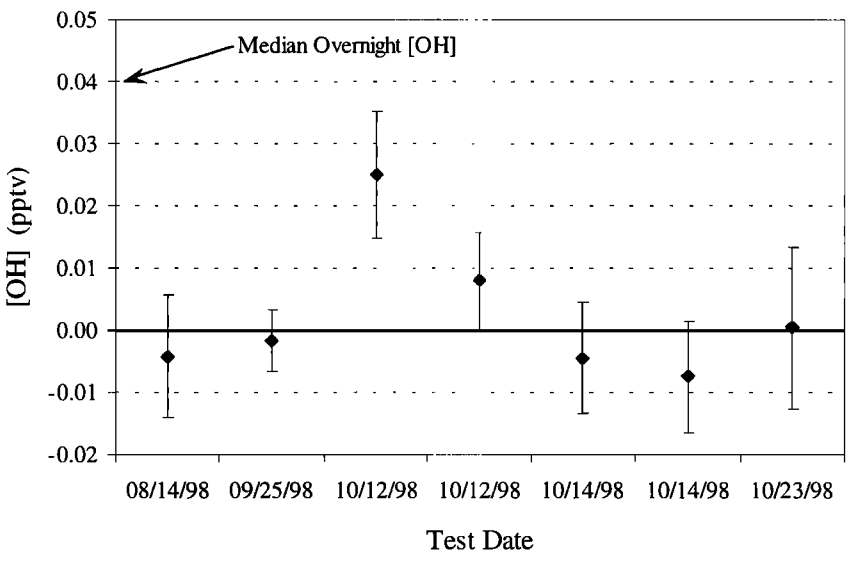

Figure 3. Average OH concentrations measured during seven different zero-air tests of the Penn State LIF instrument. The error bars indicate the 1σ precision statistics calculated for the operating parameters and duration of each test. The first test was performed on August 14, 1998, at the top of the PROPHET tower, while the others were carried out in the laboratory after the experiment field deployment. Also indicated is the magnitude of the median overnight OH concentration measured during the entire PROPHET 1998 summer intensive.

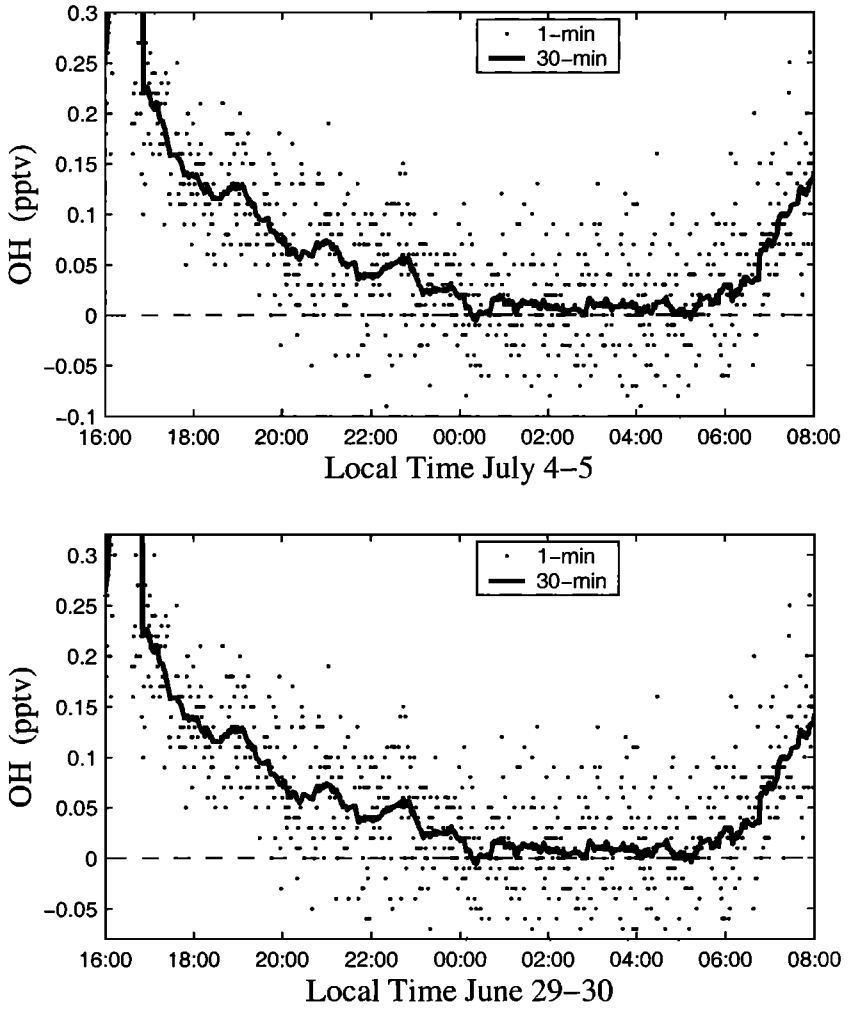

Figure 4. Time series of 1 min (dots) OH mixing ratios and 30 min running average (solid line) during two nights of the 1999 Southern Oxidant Study measured at Cornelia Fort airport outside of Nashville, Tennessee.

Nashville is presented in Figure 4. Both the 1 min data and a 30 min running average are shown for the duration of two nights in July 1999. On both nights (13 other nights of the field campaign demonstrated a similar occurrence), the 30 min average signal drops down to about 0.005 pptv (=1.2 × 10^5 molecules/cm^3) from midnight until sunrise. On the basis of Poisson statistics the precision noise of the 30 min measurements is ~0.002 pptv (= 5 × 10^4 molecules/cm^3). Thus although the overnight values are most likely statistically significant, the observed concentrations are an order of magnitude smaller than those observed at PROPHET. While the atmospheric composition of the Nashville experiment was drastically different from that of northern Michigan, the more polluted conditions of the former should be more likely to render a spurious signal due to an unknown analyte (e.g., some photolabile oxygenated hydrocarbon) if such an interference existed.

3. Nighttime Observations

A total of 720 OH and 934 30 min HO_2 data points were submitted for the 7 week PROPHET summer intensive; 40% of these data were recorded during the nighttime hours, defined here as the period when the Eppley UV-B radiometer measured zero flux. This criterion was usually met between the hours of 1930 and 0430 local mean solar time. Figure 5 is a composite of the observations of OH, HO_2, isoprene, and NO for the entire experiment along with the median diurnal profile of each species. The axis limits on these plots omit some of the observations so that a close perspective is maintained on the diurnal pattern. Several striking features of the chemical environment are evinced by these data. First, the amplitude modulation factor of the OH diurnal profile is only about 4, and a median concentration of 0.04 pptv (~10^6 molecules/cm^3) is sustained throughout the nighttime hours. The OH median curve is accompanied by dashed lines representing the ± 1σ precision of each 30 min data point, estimated to be about 0.02 pptv (~5 × 10^5 molecules/cm^3). The median observed nocturnal OH levels are therefore twice as large as the instrumental precision; however, the scatter in the individual 30 min data shown in Figure 5 represents atmospheric variability as well as instrumental noise. Second, the median isoprene profile demonstrates a precipitous decline directly following sunset from 1920 to 2120 local mean solar time (2100-2300 EDT), followed by a more gradual decay until about an hour prior to sunrise (0320 local mean solar time = 0500 EDT). The corresponding isoprene lifetimes for these two distinct decay regimes of the median

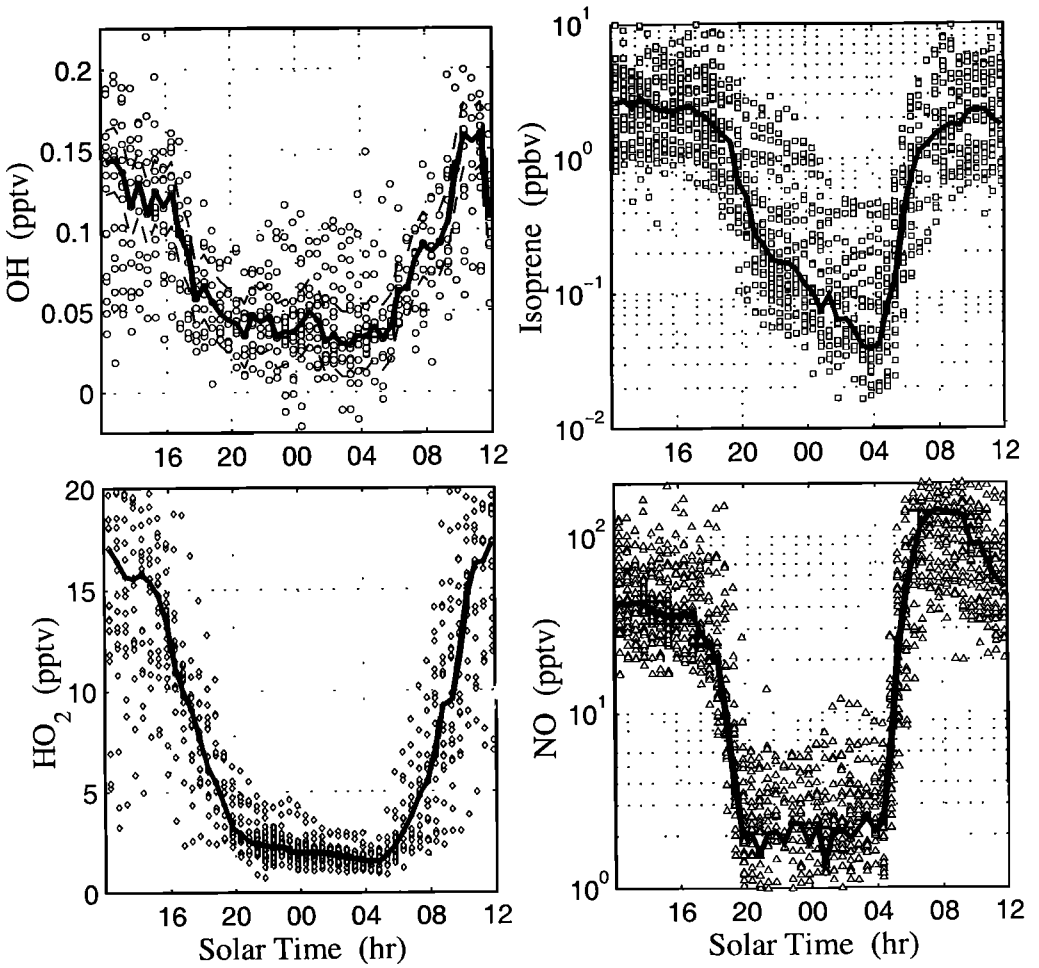

Figure 5. Composite plot of all measurements of OH (circles), HO_2 (diamonds), isoprene (squares), and NO (triangles) made during the summer intensive at the Pellston, Michigan, PROPHET research site. Each species is accompanied by a trace through the median values of each 30 min interval. The dashed lines bracketing the OH median profile represents the $\pm$ 1σ precision limits of the individual measurements. Each data point represent 30 min averages and are not all included in each axes so that the diurnal pattern could be accentuated. Local mean solar time is 100 min behind local time (EDT).

profile are 80 and 220 min, respectively. This behavior is not limited to the median profile but was consistently observed on almost all nights in which measurements were made. Third, between dusk and dawn (1930 to 0430) there is, on average, only 2 pptv of NO present, indicating small local emissions of NO_x overnight.

Figure 6 is a hybrid surface/contour plot of the diurnal median particle size spectrum measured by both TSI instruments. The diurnal profile exhibits a distinct local maximum of particle number concentration between 40 and 100 nm in diameter during the late evening hours between 2100 and midnight local mean solar time. Perusal of the wind data does not reveal any diurnal wind pattern to suggest an advected source of these small aerosols, and the winds were generally light during this period averaging less than 2.5 m/s. The peaked feature in the aerosol size spectrum also possesses a tilt toward larger sizes with time possibly indicating particle growth during this period. Aerosol dynamics such as this suggests that an ample pool of lower volatility precursor gases is present at late hours. Such condensable gases are likely to be homogeneous oxidation products; therefore Figure 6 may indicate another sign of prodigious oxidation occurring in the nocturnal boundary layer. If the population of nuclei mode aerosols is indeed growing at night, the effect could have ramifications for the ultimate fate of new CN formed by gas-to-particle conversion. For example, growth into the accumulation mode would move ultrafine aerosols into size ranges where scavenging by other aerosols is less likely, thereby increasing the lifetime of these incipient particles.

Leaitch et al. [1999] observed a similar occurrence of nocturnal particle production of diameters 60-100 nm at the Kejimkujik site in Nova Scotia, Canada. They proposed that the primary mechanism responsible for the increase in aerosols of these sizes was the oxidation of terpenes by reaction with ozone [*Atkinson*, 1997]; however, they were unable to attribute the entire loss of β-pinene (and other biogenic VOCs) to ozonolysis alone. Whether the apparent particle growth at the PROPHET site is due to ozone or hydroxyl reaction, it is indicative of considerable oxidation in the nighttime boundary layer.

3.1. Isoprene Decays and Observed OH

There are a number of indirect indications in the PROPHET 98 data set to suggest that the elevated OH

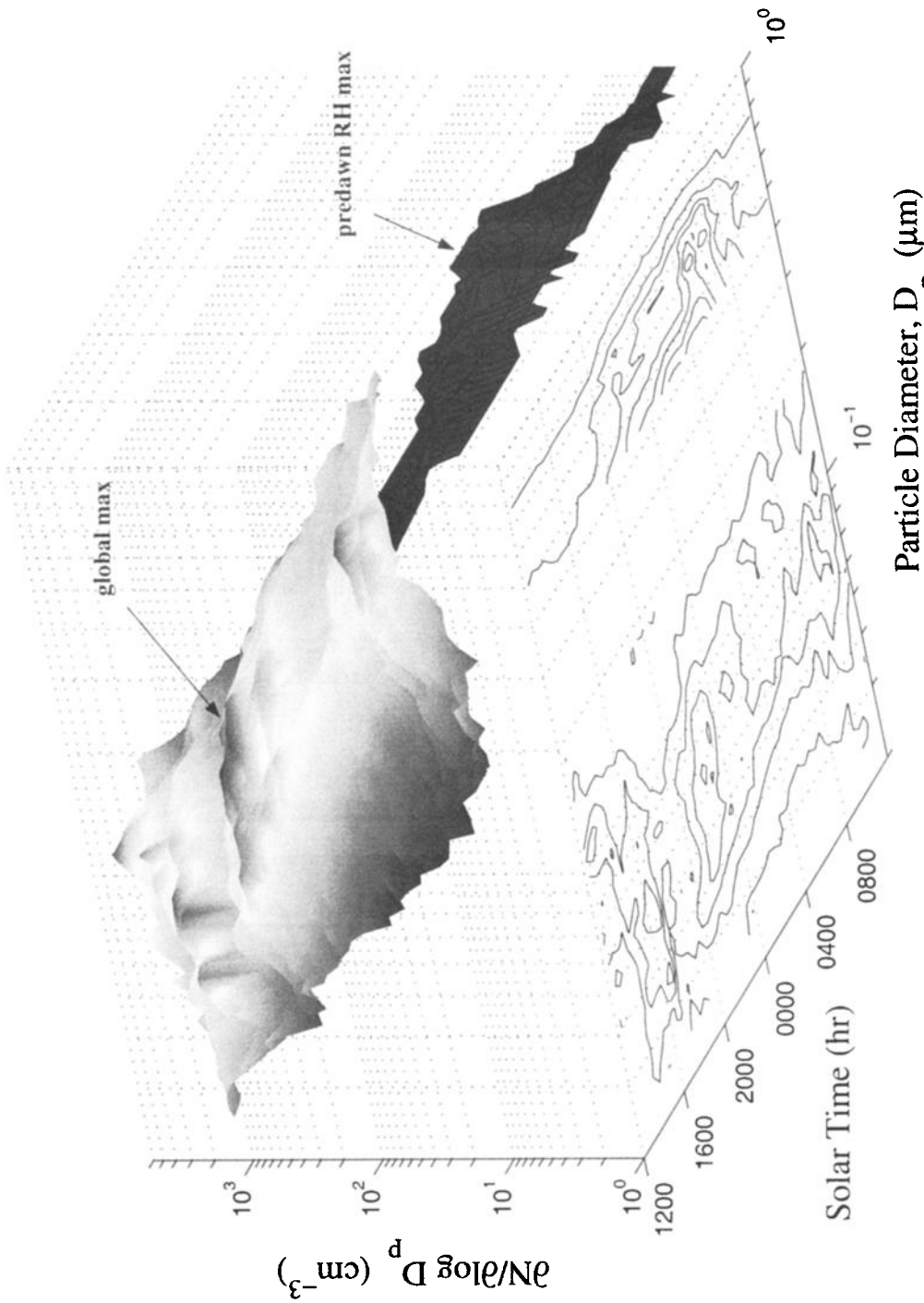

Figure 6. Diurnal median aerosol size spectrum. The *z* axis is the number density distribution – the particle number density normalized by the logarithmic width of the diameter bin. The Aitken nuclei (top surface) were measured with a TSI model 3934U scanning electrical mobility particle sizer. The larger aerosol (lower, darker surface) were measured separately with a time of flight TSI model APS3320 instrument. The number concentrations are the median values for each 30 min interval of the day. Below the surface plots are corresponding contours to illustrate the gradients more clearly.

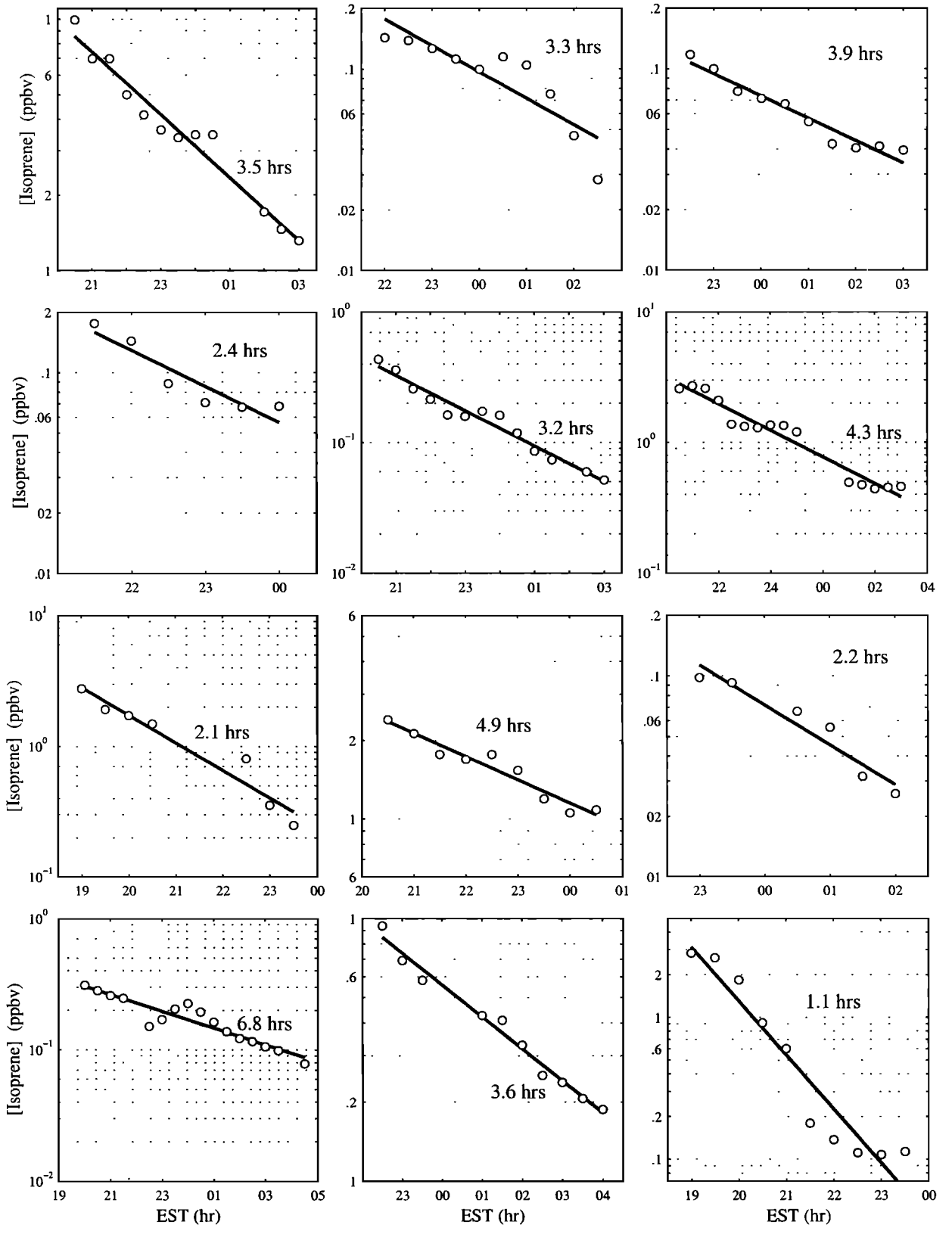

Figure 7. Twelve intervals used in the determination of the isoprene decay rates from the Purdue gas chromatograph/mass spectrometer (GC/MS) data set. The circles are the 30 min observations, and the least squares linear fit (solid lines) determines the average lifetime for the interval shown in hours in each plot.

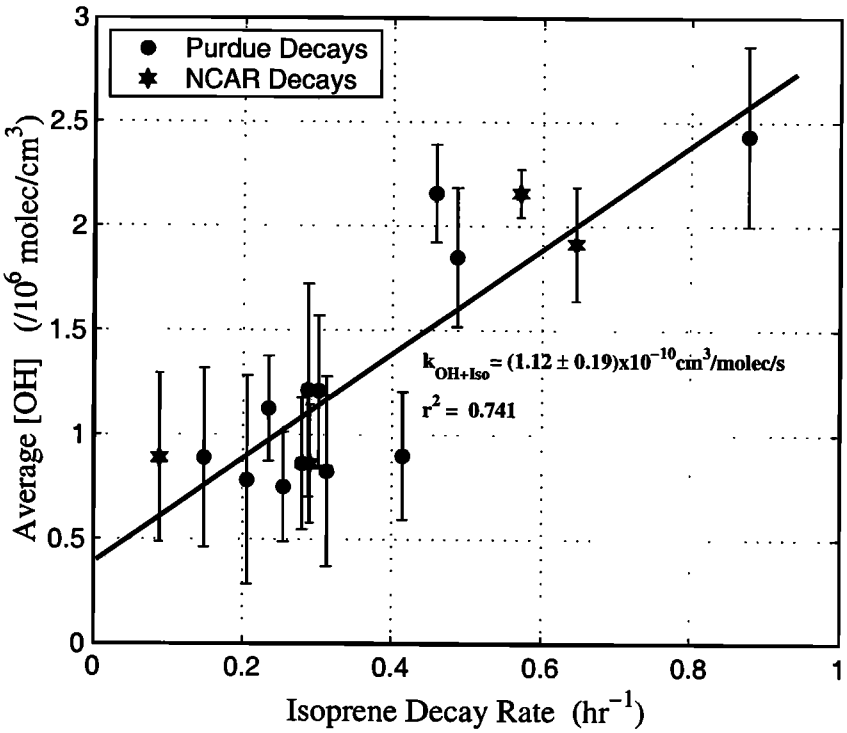

Figure 8. Measured isoprene lifetimes plotted against the OH concentrations for the corresponding interval. Along with the Purdue decays (solid circles) of Figure 7, the four nighttime decays measured by the NCAR instrument (solid stars) are also shown here. The error bars represent the combined error of the OH measurement precision and the atmospheric variability for the period of each decay.

measurements made during the night are authentic, but none are as compelling as the isoprene decays. Several researchers in a variety of forested environments have encountered anomalously fast isoprene decay rates after sunset [*Goldan et al.*, 1995; *Biesenthal et al.*, 1998; *Hurst et al.*, this issue]. Figure 7 shows 12 examples of the isoprene evening decays measured at PROPHET by the Purdue University group and the least squares fit to the decays in semilog coordinates. These nighttime decays, along with four others measured by the NCAR instrument, are plotted against the observed OH abundances for the corresponding intervals in Figure 8. The decay intervals were selected on the basis of best data overlap

Table 2. Evening Isoprene Decays

Instrument	Number	Julian Day	Start (Local Mean Solar Time)	Stop (Local Mean Solar Time)	Lifetime, τ (min) Observed	r^2	NO_3[a]	OH	Wind Direction[b]
Purdue	1	203	1950	0220	209	0.96	511*	134	88
	2	207	2120	0150	199	0.76	555*	136	15
	3	209	2150	0220	236	0.94	565*	217	98
	4	210	2050	2320	145	0.86	529*	181	252
	5	212	1920	0220	192	0.96	526*	196	76
	6	215	1950	0420	256	0.95	485*	145	284
	7	215	1820	2250	124	0.94	627*	90	243
	8	216	1920	2350	292	0.94	522*	211	92
	9	217	2220	0120	131	0.92	175	76	144
	10	222	1920	0350	407	0.88	769	183	90
	11	225	2150	0350	215	0.98	434	187	196
	12	225	1820	2320	68	0.92	614*	68	51
NCAR	13	218	0400	0700	105	0.96	175	76	144
	14	219	0030	0500	93	0.93	339	86	335
	15	223	0100	0930	688	0.81	769	183	90
	16	225	0330	0930	207	0.97	434	187	196

[a]Nitrate levels were calculated using median diurnal profiles for the hours of the decay when missing observations precluded a complete box model calculation.

[b]The average wind direction was computed by averaging the sine and cosine components of each observation, weighted by the wind speed, and then reconstructing a direction from the mean components. The direction convention is that zero degrees is a southerly wind and the angle increases counter-clockwise.

and the exclusion of periods of dramatic changes in wind direction. In an attempt to minimize the impact of variable advection in the overnight profiles, only intervals in which the wind direction changed less than 90° (and in most cases the change was less than 30°) in any 30 min were included in the analysis. Table 2 provides the intervals, linear regression statistics of the isoprene decays, wind direction, and the expected chemical lifetimes from reaction with both OH and NO_3 for the decays of Figures 7 and 8. If, as a first approach, one assumes that the late night isoprene disappearance is controlled only by chemical oxidation by OH and that all other sources or sinks of isoprene are negligible, then the correlation in Figure 8 is simply described by the reaction rate between OH and isoprene. In fact, the least squares fit to the data for Figure 8 yields a slope corresponding to a reaction rate coefficient of 1.12×10^{-10} cm^3/molecules/s. This value is well within the uncertainty limits of the rate coefficient measured by *Stevens et al.* [1999] for the average conditions of the nocturnal environment during the experiment (294 K and 998 hPa). Despite this remarkable correspondence, the linear fit does possess a positive y intercept at 3.9×10^5 molecules/cm^3, although its statistical significance is marginal.

Support of the OH measurements by the observed isoprene decays is only valid if other influences are insignificant. A complete discussion of all of the factors affecting the time evolution of the isoprene concentration may be found in the work of *Hurst et al.* [this issue]. The most likely candidates for complicating the analysis above are atmospheric mixing and competing oxidative loss by nitrate radicals. There does not appear to be any relationship between the magnitude of the decays and the prevailing wind direction nor the atmospheric stability which suggests that horizontal advection and vertical mixing are most likely not driving the overnight isoprene decays. A more complete discussion of these matters is presented in the works of *Hurst et al.* [this issue] and S. Sillman et al. (unpublished data, 2001).

Chemical transformation of isoprene by other reactive species present overnight might affect the results of Figure 8. Isoprene is known to react rapidly with ozone and the nitrate radical as well as with hydroxyl [*Atkinson*, 1997]. The reaction with ozone is not believed to be important on the timescales of interest because the lifetime of isoprene with respect to ozonolysis is over a day at the median evening ozone concentration of 37 ppbv. Nitrate was not measured at the site but is expected to be present in very small quantities due to the relatively low NO_x conditions of the environment (see Table 2). Model estimates of NO_3 indicate that the evening median value of this reactive species was only 2.1 pptv, corresponding to an isoprene lifetime of over 9 hours. By comparison, the lifetime with respect to the median hydroxyl concentration of 10^6 molecules/cm^3 is only 2 hours and 45 min; therefore the overnight isoprene decays are most likely not heavily controlled by nitrate oxidation. Details of the steady state model used to estimate the NO_3 concentrations are presented in the following section.

One last complicating factor in the OH and isoprene decay relationship is the possibility of nighttime emissions of isoprene. *Guenther* [1999] estimates that there possibly exists a nonenzymatic source of isoprene from foliage in the dark of anywhere from 1 to 100 ng/g/h in magnitude. Extensive surveys of isoprene emitters in the area surrounding the PROPHET site (mostly aspen and oak) have measured a foliar density in the area of about 155 g/m^2 (H. Westberg, personal communication, 1999). Thus an estimate of the nighttime emission strength is in the range of about 0.2-16 μg/m^2/h as opposed to a midday maximum of 5 mg/m^2/h. If the offset in Figure 8 is significant, then it points to a steady state that might be established between isoprene emissions on the one hand, countered by OH (and to a lesser extent NO_3) consumption in the dark. In fact, the median profiles of isoprene seem to illustrate just such a steady state, as the concentration tends to plateau for about 1 hour before sunrise (0320-0420) at levels between 20 and 400 pptv (Figure 5). Using the combination of the intercept in Figure 8 and the median overnight NO_3 estimation, a total chemical consumption rate of isoprene is calculated to be 8.3×10^{-5} s^{-1}. Assuming a nominal nocturnal boundary layer (NBL) height of 100 m yields an expected emission rate of ~2-30 μg/m^2/h which is in general accord with the estimate of *Guenther* [1999]. The net effect of a nocturnal emission rate unaccounted for in the foregoing analysis is that the actual chemical decay would be greater than inferred from a simple least squares estimation, and the points of Figure 8 would shift to the right by an amount proportional to the source strength. On the other hand, the presence of nitrate radicals has the opposite effect as an isoprene source. Competing oxidation would tend to shift the data of Figure 8 to the left and might be working to cancel out any emission influence.

4. Model Results and Discussion

Two different types of models used to investigate the nocturnal chemistry of the site are presented herein. The first is a steady state model of the nitrate radical concentrations. An accurate estimate of the nitrate radical abundances is crucial to the assertion that OH is the main oxidizing species in the nighttime boundary layer and therefore responsible for the isoprene decays. The second calculation is that of a zero-dimensional, steady state model which iterates the main production and loss reactions in the HO_x budget until self-consistent solutions for the OH and HO_2 concentrations are obtained. We have opted to use a very simple chemical mechanism because of the unique conditions of the study, and because our present aim is no more than to investigate some of the rudimentary possibilities and consequences of large OH production rates in the dark. The very low concentrations of NO overnight at PROPHET reduce the efficacy of models containing a "complete" chemical mechanism to capture the true chemistry. This is primarily due to the considerable dubiety surrounding many of the peroxy radical self and cross (so-called permutation) reactions as well as the mechanistic details of ozonolysis reactions [*Carter and Atkinson*, 1996].

4.1. Nitrate Radical Estimation

It has been established for over two decades that significant levels of nitrate radicals can build up at night, when they are shielded from the Sun, maintaining the atmosphere's oxidizing capacity overnight under sufficiently high NO_x conditions [*Okita*, 1976; *Platt et al.*, 1981]. Measurements and models have since been used to study the atmospheric lifetimes of NO_3 in a variety of environments [*Platt et al.*, 1990; *Smith et al.*, 1995; *Heintz et al.*, 1996]. Under the low-NO_x conditions encountered during the PROPHET 1998

intensive, the nitrate chemistry becomes essentially uncoupled from the HO_x reactions in the night. Therefore a simple steady state calculation is possible to estimate the nitrate abundance, which is independent of the HO_x levels, at each time step. Table 3 shows all of the reactions used in the estimation of the nitrate levels listed in their order of average importance for the nocturnal conditions of this experiment. Because of the importance of nitrate losses to reactions with terpenes, the nitrate calculation was only run for the subset of the campaign in which these compounds (specifically the pinenes) were measured. Reactions (R10)-(R13) represent the total nitrate losses to reactions with NO_2, including net hydrolysis of dinitrogen pentoxide (N_2O_5) from both heterogeneous and homogeneous processes. Because the dissociation of N_2O_5 back to NO_3 is on average 25 times faster than the combined hydrolysis loss rates the net loss to N_2O_5 can be approximated by [*Li et al.*, 1993]

$$L_{NO_2}^{NO_3}=[NO_2]\{k_{-10}+(\frac{k_{10}}{k_{-10}})(k_{12}+k_{13}[H_2O])\}. \quad (2)$$

Considering the rest of the reaction scheme of Table 3, the steady state nitrate concentration may be calculated:

$$[NO_3]_{ss}=\frac{k_5[O_3][NO_2]}{L_{NO_2}^{NO_3}+L_{pinenes}^{NO_3}+L_{aldehydes}^{NO_3}+L_{hetero}^{NO_3}+k_8[\text{Isoprene}]+J_{NO_3}}, \quad (3)$$

where the other losses are

$$L_{pinenes}^{NO_3}=k_7^{\alpha}[\alpha\text{-pinene}]+k_7^{\beta}[\beta\text{-pinene}], \quad (4)$$

$$L_{aldehydes}^{NO_3}=k_{15f}[HCHO]+k_{15a}[CH_3CHO], \quad (5)$$

$$L_{hetero}^{NO_3}=\sum_{i=1}^{103}\left[\frac{1}{\frac{r_i}{D_g}+\frac{4}{\gamma\bar{c}}}\right]4\pi r_i^2 N(r_i) \quad (6)$$

and r_i is the average radius of the particles in a given size range i (103 size bins ranging from 0.005 to 19.8 μm), D_g is the gas phase diffusion coefficient (=0.05 cm^2/s for NO_3), γ is the uptake coefficient, $\bar{c}$ is the mean molecular speed, and $N(r_i)$ is the aerosol number concentration distribution. Equation (6) is the integrated rate coefficient for gas phase plus interfacial mass transport as described by *Schwartz* [1986] and was used for calculation of direct heterogeneous nitrate radical and dinitrogen pentoxide (as well as hydroperoxy radical) losses.

The entire size range was not directly measured at the PROPHET site. In fact, the particle size range from 0.19 to 0.30 μm, which usually carries the statistical mode of the surface area, lies between the size resolution limits of the two instruments. It has been illustrated by other researchers that the aerosol surface area concentration can have a strong influence on the steady state NO_3 levels [*Li et al.*, 1993; *Dentener and Crutzen*, 1993; *Starn et al.*, 1998], therefore an accurate estimation of $N(r_i)$ was attempted. Because the data overlap of the two particle size instruments along with the pinene measurements amounted to only 5 days, the interpolated particle concentrations were obtained for a diurnal median profile (Figure 6). Each data set was binned into 0.5 hour averages for the complete diurnal cycle and the median profile of the interpolated size bin was applied to the entire data set.

Continental aerosol distributions can usually be approximated in the size range of interest as

$$\frac{dN}{d\log D_p}=CD_p^{-\beta}, \quad (7)$$

where D_p is the particle diameter, C is a constant related to the absolute concentration of particles, and β is a parameter between 3 and 4 for continental aerosols [*Pruppacher and Klett*, 1997]. The median data from the large end of the scanning mobility analyzer (0.15 μm<D_p<0.19 μm) is then connected by a least squares fit to the median data from the small end of the TSI time-of-flight instrument (0.35

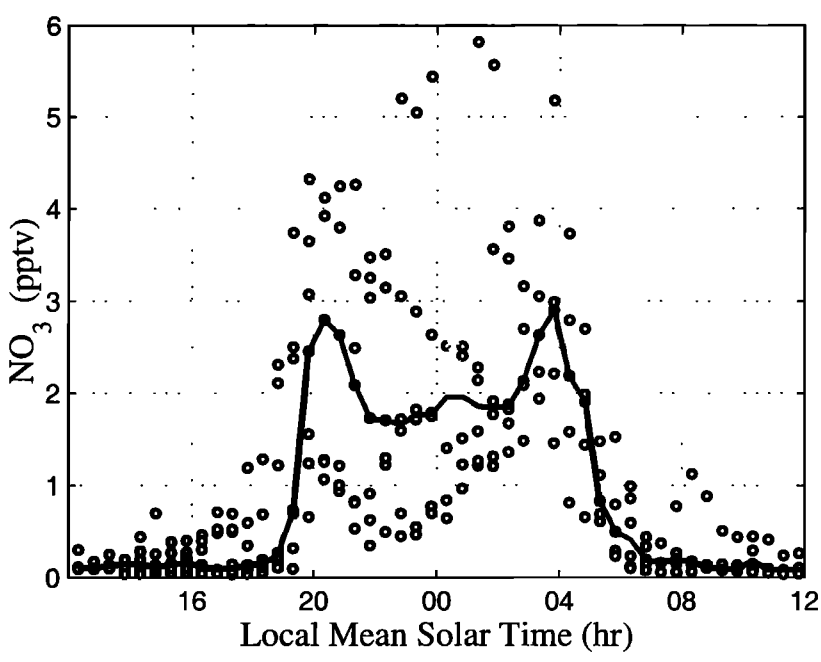

Figure 9. Median calculated NO_3 diurnal profile. Open circles are individual calculated steady state concentrations, and the solid line runs through the median values of each 30 min bin.

Table 3. Nitrate Chemical Reaction Scheme Ranked by Nighttime Importance

Reaction Number	Reaction	Rate Coefficient (Parameterization or Average Value)	Reference	% of Total Prod/Loss
	Production			
(R5)	$NO_2 + O_3 \rightarrow NO_3 + O_2$	1.2×10^{-17} exp(-2450/temp)	*DeMore* [1987]	100
	Losses			
(R6)	NO_3 + aerosol $\rightarrow NO_3^-$ (?)	$\gamma = 1.0$; mean k_6=.005 s^{-1}	*Li* [1993]	28.0
(R7)	NO_3 + pinenes $\rightarrow$ (?)	α=1.19×10^{-12} exp(490/temp); β=2.51×10^{-12}	*Atkinson* [1997]	25.9
(R8)	NO_3 + Isoprene $\rightarrow IsoONO_2$	3.0×10^{-12} exp(-446/temp)	*Atkinson* [1997]	20.0
(R9)	$NO_3 + NO \rightarrow 2NO_2$	1.7×10^{-11} exp(150/temp)	*DeMore* [1987]	15.9
(R10)	$NO_2 + NO_3 + M \Leftrightarrow N_2O_5$	1.28×10^{-12} ; $K_{eq} = 2.7 \times 10^{-27}$exp(11,000/temp)	*DeMore* [1987]	
(R11)	$NO_2 + NO_3 \rightarrow NO + NO_2 + O_2$	4.0×10^{-14} exp(-1180/temp)	*Cantrell* [1990]	
(R12)	N_2O_5 + aerosol (aq) $\rightarrow 2HNO_3$ (aq)	$\gamma = 0.05$; mean k_{12}=5.6×10^{-4} s^{-1}		
(R13)	$N_2O_5 + H_2O$ (g) $\rightarrow 2HNO_3$ (g)	1.3×10^{-21}	*Mozurkewich and Calvert* [1988]	8.6
(R14)	$NO_3 + h\nu \rightarrow NO + O_2$	mean $J_{NO_3} = 2.1 \times 10^{-4}$ s^{-1}	*Tan* [this issue]	0.8
(R15)	NO_3 + aldehydes $\rightarrow HNO_3 + RO_2$ ...	f, formaldehyde=5.8×10^{-16}; a, acetaldehyde=1.44×10^{-12} exp(-1862/temp)	*Atkinson* [1997]	0.8

$\mu m < D_p < 1.1$ μm). The diurnal pattern of β ranges from 2.9 to 3.6 with a minimum in the predawn hours when the relative humidity is greatest. This is explained by the fact that the larger aerosol number concentrations follow the diurnal pattern of relative humidity, while the smaller ones (<0.2 μm) do not (see Figure 6). The slope that connects the two size distributions then becomes less steep when the larger-particle counts are greatest in the early morning due to swelling at high humidity. The spectra thus obtained were then integrated according to equation (6) to determine the surface reaction rate coefficients for both N_2O_5 hydrolysis and direct NO_3 uptake onto aerosols. The mean surface area concentration for the evenings of the nitrate study was 284 $\mu m^2/cm^3$ corresponding to a mean particle diameter of 0.18 μm.

The nitrate concentrations were calculated using equation (6) for each 30 min time step (limited to the intervals in which pinene data were available). The resulting diurnal median profile is shown in Figure 9. The pattern that emerges from the figure is one of two distinct radical peaks during the night, which is very similar to the most frequently observed pattern of NO_3 by experimenters in the San Joaquin Valley of California [*Smith et al.*, 1995]. The difference between the environments, however, is that in the Southern California case, the NO_3 is titrated away by a buildup of local NO emissions in a shallow NBL, while in northern Michigan, it is the pinenes that shorten the NO_3 lifetime from dusk until dawn. The median nighttime concentration of the nitrate radical estimated is 2.1 pptv (using unity uptake efficiency of NO_3 on aerosols (compare Table 3). An alternate calculation using an uptake coefficient 5000 times smaller [*DeMore*, 1997] (for pure liquid water at 273 K) resulted in a median estimate of 2.9 pptv; therefore the general results are not strongly dependent on the direct aerosol loss rate.

4.2. Model HO_x Estimate

Having presented the evidence for high levels of OH in the nocturnal boundary layer, we turn to the proposal of a mechanism that can sustain such radical levels throughout the night and which is in accord with current theory and the collocated measurements. The fact that the median NO_3 concentration is estimated to be about 2 pptv, and the observed NO is, on average, just slightly over 2 pptv, implies that the fast coupling which usually describes the HO_x family [*Brune et al.*, 1998] is not at play in this environment. Because of the impeded rate of reaction (R3), as well as other known HO_2 reduction reactions (e.g., via O_3 and NO_3), any HO_x source posited to explain the observations must be a direct source of OH. Past modeling studies of nocturnal chemistry [*Bey et al.*, 1997; *Platt et al.*, 1990] have suggested that hydroxyl levels could reach from 5×10^4 to 5×10^5 molecules/cm^3 (0.002-0.02 pptv) under certain conditions (requiring concentrations of NO_x 1-3 orders of magnitude higher than in the present experiment). The only other published observations of OH at night [*Tanner and Eisele*, 1995] indicated levels of the order of 10^4 molecules/cm^3; however, these measurements were made under the relatively pristine (hydrocarbon and NO_x free) chemical conditions of the Mauna Loa Observatory in Hawaii and do not seem directly comparable. On the other hand, *Kanaya et al.* [1999] report measurements of HO_2 overnight on Oki Island which are greater than expected and propose a nighttime ozone/alkene scheme to explain the elevated HO_x.

Well before the Japanese study, however, several researchers had suggested that reactions between ozone and alkenes could represent a significant source of OH in the atmospheric boundary layer [*Atkinson et al.*, 1992; *Paulson and Orlando*, 1996]. Because these reactions have been observed to generate OH radicals directly [*Donahue et al.*, 1998] and to possess very fast rates for many biogenic hydrocarbons [*Paulson et al.*, 1998], this reaction seems to be the most likely candidate for a nocturnal HO_x source in the low-NO_x air of this forested environment. The problem with such a hypothesis has to do with the radical termination rate as illustrated in Figure 10. The loss rate of OH is believed to be well characterized by the measurements of isoprene, CO, NO_2, ozone, formaldehyde, and acetaldehyde. Together, these reactions comprise over 90% of the total instantaneous OH loss rate, estimated to be ~3.8 s^{-1}, on average, overnight at the site. The measurement of these OH loss rates puts marked constraints on hypothetical source strengths required to explain the observations. To wit, in order to maintain a level of 1×10^6 molecules/cm^3 OH, a direct OH source of 3.8×10^6 molecules/cm^3/s is needed; fewer than 2×10^5

Table 4. Model Scenarios and Median Conditions

Scenario	k_{O3} (cm³/molecules/s)	P_{terp} (molecules/cm³/s)	Production Rate[a] OH	Production Rate[a] HO_2	Deviation Ratio[b] OH	Deviation Ratio[b] HO_2	IsOO (pptv)
1	0	0	0.099	0.079	46	2.4	0.3
2	3×10^{-16}	1.4×10^{5}	0.33	0.20	15	1.0	0.5
3	1×10^{-14}	4.7×10^{6}	5.2	2.6	1.1	0.21	1.6
4	1×10^{-14}	4.7×10^{6}	4.9	4.4	1.2	0.70	85
5	1×10^{-14}	4.7×10^{6}	5.0	2.6	1.1	0.35	2.2

[a]Units of 10^6 molecules/cm³/s.
[b]Deviation ratio is defined as the observed OH divided by the model prediction, and the value reported is the arithmetic mean, whereas the other columns are median values.

molecules/cm³/s is furnished by known ozonolysis (from isoprene and the pinenes) and HO_2 reduction reactions. Even once a source of this magnitude is hypothesized, it becomes obvious that the reaction products will begin to well up into the peroxy radical pool (HO_2 + RO_2) at a very rapid pace, unless the sinks of these species concomitantly accelerate. The theoretical overnight OH production mechanism is perforce a substantial HO_2 source and, consequently, pulls the steady state estimates of the latter well above the measured levels.

Five separate model scenarios were run to investigate the possible causes of the observed HO_x levels at night (Table 4). The box model solves for both OH and HO_2 independently making an assumption of steady state, namely,

$$[X] = P_X/L_X\,, \tag{8}$$

where $[X]$ is the concentration of a particular species X, and P_X and L_X are the production and loss rates, respectively. Although the HO_x production rates in the dark should be considerably slower than in the daytime, their extreme reactivity should keep the radicals in steady state on 30 min timescales. This does become questionable for low levels of HO_2, because its lifetime with respect to self-reaction, its primary loss mechanism in this environment, at 2 pptv is just under 1 hour. The model calculates the steady state HO_x

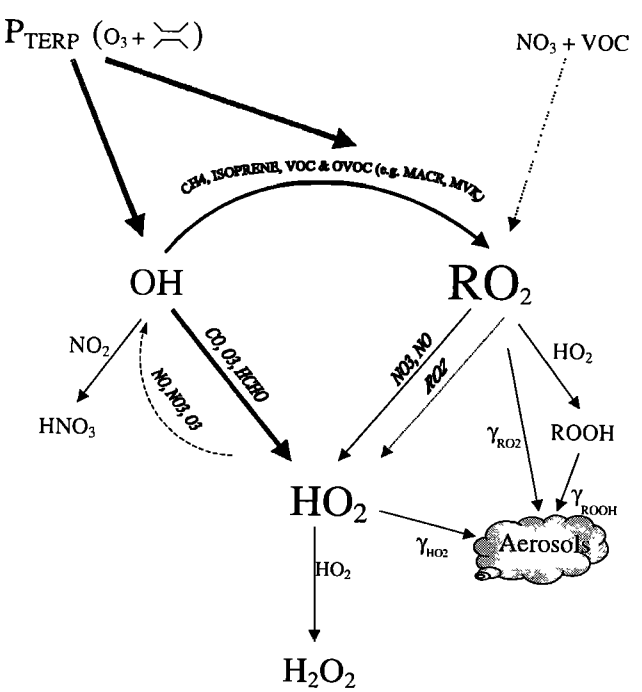

Figure 10. Schematic representation of the nighttime radical chemistry at PROPHET.

Table 5. Measured Parameters Pertinent to the Nighttime Chemistry Study and Their Median Overnight Values

Species	Experimenter Institution	Median Overnight Value Units
O_3	U. of Michigan	37 ppbv
CO	U. of Michigan	170 ppbv
NO	U. of Michigan	2.1 pptv
NO_2	U. of Michigan	780 pptv
NO_y	U. of Michigan	1.4 ppbv
RH	U. of Michigan	80 %
Temperature	U. of Michigan	294 K
Pressure	U. of Michigan	998 hPa
Isoprene	Purdue/NCAR	0.14 ppbv
Formaldehyde	Purdue	2.2 ppbv
Acetaldehyde	NCAR	570 pptv
Acetone	NCAR	2.1 ppbv
Methacrolein, MACR	NCAR	31 pptv
Methyl Vinyl Ketone, MVK	NCAR	42 pptv
3-Methylfuran, MFUR	Purdue	<MDL
Peroxyacetylnitrate, PAN	W. Michigan U.	110 pptv
α-Pinene	NCAR	13 pptv
β-Pinene	NCAR	26 pptv
Δ^3-carene	NCAR	4 pptv
Tricyclene	NCAR	4 pptv
Camphene	NCAR	3 pptv
Limonene	NCAR	2 pptv
γ-Terpinene	NCAR	2 pptv
Myrcene	NCAR	<MDL
1,8-Cineol	NCAR	<MDL
α-Phellandrene	NCAR	<MDL
Aitken particles (D<182 nm)	Michigan Tech	2,900 cm⁻³
Large particles (D>.5 mm)	U. of Michigan	17 cm⁻³

<MDL means the median value was below the instrumental limit of detection.

concentrations as well as five other unmeasured species: the NO_3 (see section 4.1), methylperoxy, acetylperoxy, and isopreneperoxy radicals, as well as peroxynitric acid (HNO_4). The other important species used in the model were constrained to the observations at each 30 min interval where data were available. Table 5 summarizes the chemical species and physical parameters used in the model along with their median overnight values. Methane was not measured, but assumed constant at 1710 ppbv. The model was run only for the evening hours, defined by zero-measured UV-B flux and compared to the observations of OH and HO_2 for those periods only. Daytime observations and model comparisons are discussed by *Tan et al.* [this issue]. The calculation of the above species is iterated until the estimated OH and HO_2 concentrations differ from their antecedents by less than 0.5%. Convergence to this threshold was usually achieved in less than 25 iterations.

The chemical scheme and kinetic parameters encoded in the model are presented in Table 6. The mechanism is limited to species that were measured at the site, in addition to the five species calculated as described above using equation (8). Most of the reaction parameters are from *DeMore et al.* [1997] and *Atkinson* [1997], but the exceptions are noted in the table. The surface area available for heterogeneous reaction was determined using the interpolated aerosol data as discussed in the nitrate radical modeling section. To ensure that the simplified chemical mechanism used was not drastically deficient, a comparison was made between the base model run and the one using a much more complete mechanism [*Tan et al.*, this issue] which was specifically developed for use in low-NO_x environments. The general agreement in trend was quite good, but the complete model calculated approximately 30% less OH than the simplified mechanism described here. This is not very surprising

Table 6. Nocturnal HO_x Chemical Reaction Scheme Used in Box Model, and the Median Apportionment Relative to Total Instantaneous Production and Loss for the Baseline Scenario

No.	Reaction	Ref.	%	No.	Reaction	Ref	%
	OH Loss				HO_2 Production		
(R5a)	$OH + CO \rightarrow HO_2 + CO_2$	De	42	(R5a)	$OH + CO \rightarrow HO_2 + CO_2$	De	50
(R5b)	$OH + HCHO \rightarrow HO_2 + CO + H_2O$	De	21	(R5b)	$OH + HCHO \rightarrow HO_2 + CO + H_2O$	De	30
(R5c)	$OH + O_3 \rightarrow HO_2 + O_2$	De	1.2	(R5c)	$OH + O_3 \rightarrow HO_2 + O_2$	De	1.8
(R6)	$OH + H_2O_2 \rightarrow HO_2 + H_2O$	De	0.2	(R6)	$OH + H_2O_2 \rightarrow HO_2 + H_2O$	De	0.3
(R7)	$OH + CH_4 \rightarrow CH_3OO + H_2O$	De	6.4	(R20)	$CH_3OO + NO/NO_2 \rightarrow\rightarrow HO_2 + \ldots$	Ma	7.9
(R8)	$OH + NO_2 \rightarrow HNO_3$	Dr	5.6	(R21)	$CH_3OO + CH_3OO \rightarrow\rightarrow 0.6HO_2 + \ldots$	De	NS
(R9)	$OH + HO_2NO_2 \rightarrow$ products	De	NS	(R22)	$IsOO + CH_3OO \rightarrow\rightarrow 1.25HO_2 + \ldots$	Ma	NS
(R10)	$OH + HNO_3 \rightarrow H_2O + NO_3$	De	NS	(R23)	$IsOO + IsOO \rightarrow\rightarrow 0.5HO_2 + \ldots$	Ma	NS
(R11)	$OH + C_5H_8$ (isoprene) $\rightarrow$ IsOO	At	8.4	(R24)	$IsOO + NO/NO_2 \rightarrow\rightarrow 0.9HO_2 + \ldots$	Ma	5.3
(R12)	$OH + CH_3CHO \rightarrow CH_3(CO)OO + H_2O$	A2	5.6	(R25)	$NO_3 + HCHO \rightarrow HNO_3 + HO_2$	A2	3.1
(R13)	$OH + \alpha/\beta$-Pinene $\rightarrow$ products	At	1.4				
(R14)	$OH + MACR \rightarrow$ products	Gi	1.7		HO_2 Loss		
(R15)	$OH + MVK \rightarrow$ methylvinyl peroxy	Gi	0.6	(R27)	$HO_2 + IsOO \rightarrow ROOH + O_2$	Ma	4.7
(R16)	$OH + HO_2 \rightarrow H_2O + O_2$	De	0.1	(R16)	$OH + HO_2 \rightarrow H_2O + O_2$	De	0.1
	OH Production			(R26)	$HO_2 + HO_2 \rightarrow H_2O_2 + O_2$	De	7.8
(R2a)	$HO_2 + O_3 \rightarrow OH + 2O_2$	De	40	(R2a)	$HO_2 + O_3 \rightarrow OH + 2O_2$	De	49
(R2b)	$HO_2 + NO \rightarrow OH + NO_2$	De	13	(R2b)	$HO_2 + NO \rightarrow OH + NO_2$	De	17
(R2c)	$HO_2 + NO_3 \rightarrow OH + NO_2 + O_2$	De	3.3	(R2c)	$HO_2 + NO_3 \rightarrow OH + NO_2 + O_2$	De	4.1
(R17)	$O_3 + C_5H_8 \rightarrow\rightarrow 0.68\ OH + \ldots$	At	22	(R28)	$HO_2 + CH_3OO \rightarrow CH_3OOH + O_2$	De	1 4
(R18)	$O_3 + \alpha$-Pinene $\rightarrow\rightarrow 0.8\ OH + \ldots$	At	15	(R29)	$HO_2 + CH_3COOO \rightarrow$ prods	De	0.6
(R19)	$O_3 + \beta$-Pinene $\rightarrow\rightarrow 0.35\ OH + \ldots$	At	3.2	(R30)	HO_2 + aerosol surfaces, γ=0.025	De	9 5

NS denotes a median fraction of total production or loss is not significant, < 0.1%. At, *Atkinson* [1997]; A2, *Atkinson et al.* [1997]; De, *DeMore et al.* [1997]; Ma, *Makar et al.* [1999]; Gi, *Gierczak et al.* [1997].

considering that many of the additional species contained in the former model (not constrained by observations) act as OH sinks. This indicates that the estimates made in the following discussion may represent lower limits of necessary OH source strengths to account for the observations because some of the OH sinks are not included in the model. We do not feel that this severely compromises the utility of this analysis because the purpose here is to explore some of the very simple, zero-order issues surrounding the question of whether or not it is possible to reproduce our field observations in a model given our current understanding of the chemistry.

The five model scenarios comprise first a baseline run which only includes the OH production terms measured and expected by conventional atmospheric chemistry (i.e., ozonolysis of isoprene and the pinenes with their corresponding OH yields). The second scenario prescribes an additional terpene ozonolysis source (P_{terp}) sufficient to bring the HO_2 estimates within 5% of the observed levels on average. A third model run was made with an even greater terpene source sufficient to match the observed OH levels. Although in the latter case the model closely reproduces the high levels of hydroxyl in the nocturnal system, the HO_2 amounts are on average 5 times larger than those observed. Steady state box models, such as that used herein, are inadequate to calculate accurately organic peroxy radicals in the nighttime atmosphere because these species are not expected to be in steady state. Only a diel model will be able to capture the buildup of peroxy radicals during the course of the day, and their gradual decay throughout the night. Nevertheless, in order to investigate the possibility of unmeasured radical sinks in explaining the HO_2 difference, a fourth model scenario is presented wherein the isoprene peroxy radical levels are arbitrarily inflated to greater than 90 pptv. This is equivalent to using the isoprene peroxy radical as a proxy for all organic peroxy radicals that might be formed in the proposed ozonolysis and other oxidation reactions. In addition, the fourth model run increased the uptake coefficient γ for HO_2 onto atmospheric aerosols from 0.025 to unity. The motivation for adjusting the heterogeneous reactivity by such a large degree was to see if the large HO_2 model values could be significantly reduced to be on par with the observations. Moreover, the fact that the aerosols in this forested region are likely to be coated by organic films [*Graedel and Weschler*, 1981], as argued earlier vis-à-vis Figure 6, may imply that their surface reactivities are greatly enhanced. In this way, both the isopreneperoxy radicals and the aerosol surfaces are used in the model as a possible HO_2 radical drain (see Figure 10). Finally, in order to see these effects independently a fifth run was carried out with only the HO_2 uptake coefficient set to unity and the peroxy levels calculated as usual.

The tabulated scenarios show the various HO_x production terms and observation-to-model ratios (Table 4). P_{terp}, the additional OH source, is postulated as an ozone and terpene reaction, some of which have been observed to directly generate OH [*Donahue et al.*, 1998]. The OH-producing branch of the ozonolysis mechanism is thought to proceed via the Criegee intermediate as follows:

$$O_3 + R_1HC{=}CHR_2 \rightarrow R_2CHO + \left[R_1HC^{\bullet}OO^{\bullet}\right]^{*}$$

$$\left[R_1HC^{\bullet}OO^{\bullet}\right]^{*} \xrightarrow{O_2} {}^{\bullet}OH + R_1(CO)OO^{\bullet}. \quad \text{(R31)}$$

The products of the first stage of this reaction are vibrationally excited and the $R_1HC^{\bullet}OO^{\bullet}$ Criegee biradical can easily dissociate yielding an OH radical and an oxygenated peroxy radical [*Donahue et al.*, 1998]. The peroxy radical product, if it stays in the gas phase, will further serve to exacerbate the conceptual problem of the swelling radical pool outlined earlier.

In working with the steady state model it became apparent that the requisite OH source was correlated to the product of ozone and the measured monoterpene, Δ^3-carene. For this reason the putative terpene source was scaled to this product for model runs 2-5. Incidentally, the reaction rate of ozone with Δ^3-carene is not especially rapid (3.7×10^{-17} cm^3/molecules/s) [*Atkinson*, 1997], thus its reaction with ozone is not sufficiently prolific to account for the nighttime OH. However, it may be that the relation arises from another more reactive terpene that is correlated with Δ^3-carene in the atmosphere due to, for example, similar vegetative sources. While the other products of reaction (R31) are not well characterized, they are presumably large, carbonyl compounds possessing low vapor pressures and their production after sunset might contribute to the late night peak in small particle growth illustrated in Figure 6.

Each of the model scenarios which incorporates P_{terp} arbitrarily scales the reactive terpene to Δ^3-carene such that the average overnight concentration is 18 pptv, some 3.5 times greater than the measured levels of Δ^3-carene itself. By comparison, this amount of terpene is approximately equivalent to the average nighttime α-pinene concentration measured during the campaign. Laboratory measurements of typical OH yields from these types of reactions are usually in the range of 0.1-1.0 [*Atkinson*, 1997]. Because of the speculative nature of the source we avoid postulating a realistic OH yield and assume it to be unity for the sake of argument. Much greater variability and uncertainty in P_{terp} is embodied in the rate coefficient of the supposititious reaction with ozone, thus the latter is used to control the magnitude of the hypothetical source. Model scenario 2 assumes an ozonolysis reaction rate coefficient of 4×10^{-16} cm^3/molecules/s, while scenarios 3 and 4 use 10^{-14} cm^3/molecules/s. The former rate is similar to that of the monoterpene myrcene, and the latter is less common but still observed for some cyclic diolefin and sesquiterpene compounds (e.g., α-terpinene, β-caryophyllene, and α-humulene [*Atkinson*, 1997]). The lifetime of such a reactive compound under typical nocturnal conditions at PROPHET (i.e., 37 ppbv O_3) is of the order of 2 min. Thus in order to sustain such a large hydroxyl production rate (given the same assumptions in the previous discussion about nocturnal isoprene emissions and assuming the molecular weight of a monoterpene, 136 amu) there would have to exist a terpene source strength of approximately 0.36 mg/m^2/h. Although the theoretical terpene concentration necessary to explain the elevated OH is of the order of the observed levels of α-pinene, because the lifetime is approximately 20 times shorter, the required emission strength is proportionally larger.

Two nights from the campaign are chosen to illustrate the general relationship among the observations of HO_2 and the different model runs (Figure 11). Although the general shapes of the HO_2 tendencies overnight seem to match the observations (gradual dip and recovery on August 11 and

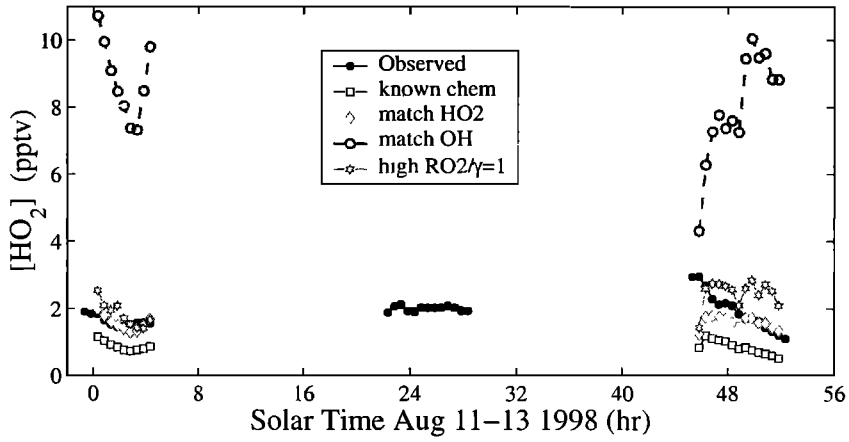

Figure 11. HO_2 observations and model estimates for the late night/early mornings of August 11 and 13 (Julian days 223 and 225). The solid circles are the measured concentrations, and the model scenarios (open symbols) are described in the text and in Table 4.

nearly monotonic decrease on August 13), the modeled amounts are acutely influenced by the magnitude of the proposed OH source. The agreement between model and observation is obviously much better in scenarios 2, with the moderate terpene source, and 4 where the P_{terp} source is large and there are sufficiently fast sinks to remove the HO_2.

The correlation between nighttime observations of OH and the model results calculated with the largest terpene source (run 3) is shown in Figure 12. The average ratio of the observed to modeled OH levels is 1.01 for this scenario. Arbitrarily scaling the additional OH source to the concentrations of ozone and Δ^3-carene seems to capture over 50% of the variability in the measurements.

To explore the possibility of another reducing agent coming into play in the HO_x cycle at the very low NO levels experienced overnight at the site, we experimented with a

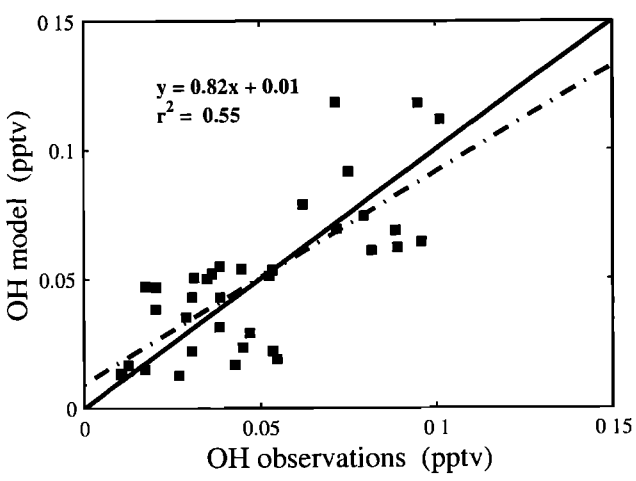

Figure 12. Observed and modeled OH for model scenario 3 in which a large terpene source of HO_x is present throughout the night. The solid squares are the 30 min measurements and the corresponding modeled value, the solid line is the one-to-one line, and the dashed-dotted line is the least squares fit to the data. There are 35 points in the comparison, and the probability that the model and measurement are uncorrelated is <.05%.

reactant presumed to have the same rate coefficient with HO_2 as NO. Putting in 200 pptv of such a reactant enabled the P_{terp} term to be reduced to 1.6×10^6 (equivalent to a reaction rate with ozone of 3×10^{-15} cm³/molecules/s, vide supra). While this model run brings both the OH and the HO_2 to within 10% of the observed values, the existence of an unknown trace species with the equivalent reduction potential of 200 pptv of nitric oxide is highly unlikely.

5. Conclusions

The explanation posited herein for the elevated nocturnal OH concentrations observed during the summer 1998 in northern Michigan involves an unmeasured, extremely reactive olefinic compound most probably a terpenoid. Given that such compounds tend to be emitted in greater quantities by coniferous trees, the hypothesis is difficult to accept given that the forest surrounding the PROPHET site is made up of ~90% deciduous species. If the hypothesis is correct, however, the chemical consequences could be even greater in boreal forests, which cover approximately 17% of the Earth's continents. Moreover, because of the predominance of these types of ecosystems in high latitudes, export of ozone to these regions could serve to reduce latitudinal gradients of OH. On the other hand, *Hurst et al.* [this issue] point out that no indications of anomalously rapid nocturnal oxidation of isoprene was observed during the BOREAS experiment in Saskatchewan, Canada, where the surrounding forest is dominated by black spruce and jack pine species.

Other possible sources of nocturnal OH most likely also involve the profligate generation of organic peroxy radicals, which leads to an abundance of such radicals as described in the body of the text. Our understanding of overnight oxidation in low-NO_x environments such as this one, is strongly contingent on a more complete understanding of the life of organic peroxy radicals and the rates of their permutation reactions. Much further investigation is required in mapping out the complete chemical mechanisms of the ozonolysis of biogenic olefinic compounds, especially under low-NO_x conditions.

Chemical ramifications of the unexpected diurnal profile of OH are difficult to assess at this stage. The timing of the

atmosphere's oxidative industry could conceivably influence the ultimate fate of many trace gases. One example was proposed in section 3 where it is argued that nocturnal oxidation might affect aerosol growth dynamics by advancing nuclei mode particles freshly formed from afternoon photochemical activity into the accumulation mode, thereby reducing the probability of their loss due to scavenging. Similarly, reactive hydrocarbons emitted into the surface layer, along with their oxidation progeny, might remain in the presence of OH for longer reaction times than expected and thus follow altered chemical pathways (e.g., variable reaction yields) which might in turn modify their atmospheric fate.

Finally, the numerical study by *Bey et al.* [1997] indicated that whatever the OH concentrations obtained in the NBL, the amounts in the residual layer above are typically 3-10 times smaller. The same type of stratification would be expected at the PROPHET site because of the short lifetimes of both the putative reactive terpene and the resultant OH. The extreme reactivity of these compounds would most likely limit the vertical extent of their impact. However, this lower layer of elevated OH would produce an active region of chemical loss near the surface, and coupled with vertical mixing, could enhance the deposition fates of many compounds.

Acknowledgments. This research was supported by NSF grants ATM-9628059-659C, -D, and -H. We would like to thank many colleagues for candid, fruitful discussions on this topic: John Wyngaard, Peter Neeb, Jim Crawford, Fangqun Yu, Hartwig Harder, Steve Bertman, and Monica Martinez. We also thank James Simpas, Jeremy Bassis, and Robert Lesher at Penn State for their consistent hard work. The first author would further like to thank the organizers and participants of the ACCESS-V meeting for their creative interrogation and support. His work on this topic was generously supported by a NASA Earth System Science Fellowship (reference 1995-GlobalCh00086.)

References

Aliwell, S. R., and R. L. Jones, Measurements of tropospheric NO_3 at midlatitude, *J. Geophys. Res.*, *103*, 5719-5727, 1998.

Atkinson, R., Gas-phase tropospheric chemistry of volatile organic compounds, 1, Alkanes and alkenes, *J Phys. Chem. Ref. Data*, *26*(2), 215-290, 1997.

Atkinson, R., S. M. Aschmann, J. Arey, B. Shorees, Formation of OH radicals in the gas phase reactions of O_3 with a series of terpenes, *J. Geophys. Res.*, *97*, 6065-6073, 1992.

Atkinson, R., et al., Evaluated kinetic, photochemical, and heterogeneous data for atmospheric chemistry: Supplement V, IUPAC subcommittee on gas kinetic data evaluation for atmospheric chemistry, *J. Phys. Chem. Ref. Data*, *26*, 521-1012, 1997.

Barket, D. J., Jr., et al., Intercomparison of automated methodologies for determination of ambient isoprene during the PROPHET 1998 summer campaign, *J. Geophys. Res.*, this issue.

Bey, I., B. Aumont, and G. Toupance, The nighttime production of OH radicals in the continental troposphere, *Geophys. Res. Lett.*, *24*(9), 1067-1070, 1997.

Biesenthal, T. A., J. W. Bottenheim, P. B. Shepson, S.-M. Li, and P. C. Brickell, The chemistry of biogenic hydrocarbons at a rural site in eastern Canada, *J. Geophys. Res.*, *103*, 25,487-25,498, 1998.

Brune, W. H., et al., Airborne in situ OH and HO_2 observations in the cloud-free troposphere and lower stratosphere during SUCCESS, *Geophys. Res. Lett.*, *25*, 1701-1704, 1998.

Cantrell, C. A., A. Zimmer, and G. S. Tyndall, Absorption cross sections for water vapor from 183 to 193 nm, *Geophys. Res. Lett.*, *24*(17), 2195-2198, 1997.

Carroll, M. A., P. B. Shepson, and S. B. Bertman, Overview of the Program for Research on Oxidants: Photochemistry, Emissions, and Transport (PROPHET) summer 1998 measurements intensive, *J. Geophys. Res.*, this issue.

Carter, W. P. L., and R. Atkinson, Development and evaluation of a detailed mechanism for the atmospheric reactions of isoprene and NO_x, *Int. J. Chem. Kinet.*, *28*, 497-530, 1996.

Cooper, O. R., J. L. Moody, T. Thornberry, M. Town, and M. A. Carroll, PROPHET 1998 meteorological overview and air mass classification, *J. Geophys. Res.*, this issue.

DeMore, W. B., S. P. Sander, D. M. Golden, R. F. Hampson, M. J. Kurylo, C. J. Howard, A. R. Ravishankara, C. E. Kolb, and M. J. Molina, Chemical kinetics and photochemical data for use in stratospheric modeling. Evaluation number 12, *JPL Publ. 97-4*, 266 pp., Jet Propul. Lab, Pasadena, Calif., 1997.

Dentener, F. J., and P. J. Crutzen, Reaction of N_2O_5 on tropospheric aerosols: Impact on the global distributions of NO_x, O_3, and OH, *J. Geophys. Res.*, *98*, 7149-7163, 1993.

Donahue, N. M., J. H. Kroll, J. G. Anderson, and K. L. Demerjian, Direct observation of OH production from the ozonolysis of olefins, *Geophys. Res. Lett.*, *25*(1), 59-62, 1998.

Dubey, M. K., T. F. Hanisco, P. O. Wennberg, and J. G. Anderson, Monitoring potential photoechemical interference in laser-induced fluorescence measurements of atmospheric OH, *Geophys. Res. Lett.*, *23*(22), 3215-3218, 1996.

Eisele, F. L. and J. D. Bradshaw, The elusive hydroxyl radical: Measuring OH in the atmosphere, *Anal. Chem.*, *65*(21), 927-939, 1993.

Faloona, I., et al., Observations of HO_x and its relationship with NO_x in the upper troposphere during SONEX, *J. Geophys. Res.*, *105*, 3771-3783, 2000.

Gierczak, T., J. B. Burkholder, R. K. Talukdar, A. Melkuki, S. B. Barone, and A. R. Ravishankara, Atmospheric fate of methyl vinyl ketone and methacrolein, *J. Photochem. Photobiol. A Chem.*, *110*, 1-10, 1997.

Goldan, P. D., W. C. Kuster, F. C. Fehsenfeld, and S. A. Montzka, Hydrocarbon measurements in the southeastern United States: The Rural Oxidants in the Southern Environment (ROSE) Program 1990, *J. Geophys. Res.*, *100*, 25,945-25,963, 1995.

Graedel, T. E., and C. J. Weschler, Chemistry within aqueous atmospheric aerosols and raindrops, *Rev. Geophys.*, *19*, 505-539, 1981.

Guenther, A., Modeling biogenic volatile organic compound emissions to the atmosphere, in Reactive Hydrocarbons in the Atmosphere, edited by C. Hewitt, pp. 97-118, Academic, San Diego, Calif., 1999.

Hard, T. M., R. J. O'Brien, C. Y. Chan, and A. A. Mehrabzadeh, Tropospheric free radical determination by FAGE, *Environ. Sci. Technol.*, *18*, 768, 1984.

Heintz, F., U. Platt, H. Flentje, and R. Dubois, Long-term observation of nitrate radicals at the Tor Station, Kap Arkona (Rugen), *J. Geophys. Res.*, *101*, 22,891-22,910, 1996.

Hurst, J. M., et al., Investigation of the nighttime decay of isoprene, *J. Geophys. Res.*, this issue.

Kanaya, Y., Y. Sadanaga, J. Matsumoto, U. K. Sharma, J. Hirokawa, Y. Kajii, and H. Akimoto, Nighttime observation of the HO_2 radical by an LIF instrument at Oki Island, Japan, and its possible origins, *Geophys. Res. Lett.*, *26*(14), 2179-2182, 1999.

Leaitch, W. R., J. W. Bottenheim, T. A. Biesenthal, S.-M. Li, P. S. K. Liu, K. Asalian, H. Dryfhout-Clark, and F. Hopper, A case study of gas-to-particle conversion in an eastern Canadian forest, *J. Geophys. Res.*, *104*, 8095-8111, 1999.

Li, S.-M., K. G. Anlauf, and H. A. Wiebe, Heterogeneous nighttime production and deposition of particle nitrate at a rural site in North America during summer 1988, *J. Geophys. Res.*, *98*, 5139-5157, 1993.

Makar, P. A., J. D. Fuentes, D. Wang, R. M. Staebler, and H. A. Wiebe, Chemical processing of biogenic hydrocarbons within and above a temperate deciduous forest, *J. Geophys. Res.*, *104*, 3581-3603, 1999.

Okita, T., Measurement of gaseous and particulate nitrates in the atmosphere, *Atmos. Environ.*, *10*(12), 1085-1089, 1976.

Paulson, S. E., and J. J. Orlando, The reactions of ozone with alkenes: An important source of HO in the boundary layer, *Geophys. Res. Lett.*, *23*, 3727-3730, 1996.

Paulson, S. E., M. Chung, A. D. Sen, and G. Orzechowska, Measurement of OH radical formation from the reaction of ozone with several biogenic alkenes, *J. Geophys. Res.*, *103*, 25,533-25,539, 1998.

Platt, U., D. Perner, J. Schröder, C. Kessler, and A. Toennissen, The

diurnal variation of NO_3, *J. Geophys. Res.*, *86*, 11,965-11,970, 1981.

Platt, U., G LeBras, G. Poulet, J.P. Burrows, and G. Moortgart, Peroxy radicals from nighttime reaction of NO_3 with organic compounds, *Nature*, *348*, 147-149, 1990.

Pruppacher, H. R., and J. D. Klett, Microphysics of Clouds and Precipitation, Kluwer Academic, Boston, 1997.

Schwartz, S. E., Mass transport considerations pertinent to aqueous phase reactions of gases in liquid-water clouds, in *Chemistry of Multiphase Atmospheric Systems*, edited by Wolfgang Jaeschke, pp. 415-471, Springer-Verlag, New York, 1986.

Smith, N., J. M. C. Plane, C.-F. Nien, and P. A. Solomon, Nighttime radical chemistry in the San Joaquin Valley, *Atmos. Environ.*, *29*(21), 2887-2897, 1995.

Starn, T. K., P. B. Shepson, S. B. Bertman, D. D. Riemer, R. G. Zika, and K. Olszyna, Nighttime isoprene chemistry at an urban-impacted forest site, *J. Geophys. Res.*, *103*, 22,437-22,447, 1998.

Stevens, P. S., J. H. Mather, and W. H. Brune, Measurement of tropospheric OH and HO_2 by laser-induced fluorescence at low pressure, *J. Geophys. Res.*, *99*, 3542-3557, 1994.

Stevens, P., D. L'Esperance, B. Chuong, and G. Martin, Measurements of the kinetics of the OH-initiated oxidation of isoprene: Radical propagation in the OH + Isoprene + O_2 + NO reaction system, *Int. J. Chem. Kinet.*, *31*, 637-643, 1999.

Sumner, A. L., et al., A study of formaldehyde chemistry above a forest site, *J. Geophys. Res.*, this issue.

Tan, D., et al., HO_x budgets in a deciduous forest: Results from the PROPHET summer 1998 campaign, *J. Geophys. Res.*, this issue.

Tanner, D. J., and F. L. Eisele, Present OH measurement limits and associated uncertainties, *J. Geophys. Res.*, *100*, 2883-2892, 1995.

Thornberry, T. D., et al., Observations of reactive oxidized nitrogen and speciation of NO_y during the PROPHET 1998 summer intensive, *J. Geophys. Res.*, this issue.

Trainer, M., E. Y. Hsie, S. A. McKeen, R. Tallamraju, D. D. Parrish, F. C. Fehsenfeld, and S. C. Liu, Impact of natural hydrocarbons on hydroxyl and peroxy radicals at a remote site, *J. Geophys. Res.*, *92*, 11,879-11,894, 1987.

Wayne, R. P., et al., The nitrate radical: Physics, chemistry, and the atmosphere, *Atmos. Environ.*, *25*(A), 1-203, 1991.

E. Apel and I. Faloona, National Center for Atmospheric Research, Boulder, CO 80304. (apel@ucar.edu; faloona@ucar.edu.)

D. Barket Jr., T. L. Couch, J. Hurst, and P. Shepson, Department of Chemistry, Purdue University, West Lafayette, IN 47907.

W. H. Brune, Department of Meteorology, The Pennsylvania State University, University Park, PA 16802. (brune@essc.psu.edu.)

M. A. Carroll, G. J. Keeler, S. Sillman, and T. Thornberry, Atmospheric, Oceanic, and Space Sciences Department, University of Michigan, Ann Arbor, MI 48109.

D. Hooper, K. Paterson, and J. Sagady, Department of Civil and Environmental Engineering, Michigan Technological University, Houghton, MI 49931.

D. Riemer, Rosenstiel School of Marine & Atmospheric Science, University of Miami, Miami, FL 33149-1098.

D. Tan, School of Earth and Atmospheric Sciences, Georgia Institute of Technology, Atlanta, GA 30332. (tan@minitower.gtri.gatech.edu.)

(Received February 9, 2000; revised September 5, 2000; accepted October 13, 2000.)